Cn2 profile characterization from wavefront sensing in moderate turbulence

Yann Lai-Tim[a], Florian Quatresooz[a], Steve Tyler[a], Mathieu Esclingand[a], Serge Meimon[a], Vincent Michau[b], Thierry Fusco[b], and Nicolas Védrenne[b]

[a]DOTA, ONERA, Université Paris-Saclay, 92320, Châtillon, France
[b]DOTA, ONERA, Université Paris-Saclay, 91120, Palaiseau, France

ABSTRACT

Atmospheric turbulence degrades the optical resolution of long range imagers and the capacity to properly focus a laser beam on a target. Assessing accurate C_n^2 profiles along the propagation line of sight yields crucial insights for tailoring adaptive optics control strategies and image processing techniques that can mitigate the effects of the atmospheric turbulence. The SCO-SLIDAR method can estimate C_n^2 profiles by exploiting both wavefront slope and scintillation correlations recorded simultaneously with a Shack-Hartmann wavefront sensor on a point source. In this paper, we present an experimental application of the SCO-SLIDAR method for turbulence profiling under near-ground, horizontal observation conditions. Using Shack-Hartmann (SH) slope and intensity measurements from unresolved sources in different directions, we reconstructed C_n^2 turbulence profiles that showed consistency across all directions. To validate the reliability of our approach, we compared macroscopic turbulence parameters (r_0 and σ_χ^2) derived from the measured profiles with those calculated directly from the SH data. The good agreement for both r_0 and σ_χ^2 confirms the technique's ability to accurately estimate the integral of the profile and distant turbulent layers, respectively. These results provide a solid foundation for future work aimed at experimentally validating anisoplanatism error in endo-atmospheric environments.

Keywords: C_n^2 profile measurement, turbulence monitoring, adaptive optics

1. INTRODUCTION

Atmospheric turbulence degrades the optical resolution of long-range imagers and impairs the ability to accurately focus a laser beam on a target. Fortunately, it is possible to perform real-time compensation of these atmospheric aberrations using adaptive optics (AO). Classic AO systems rely on a wavefront sensor to measure the turbulent phase. In solar astronomy or endo-atmospheric (i.e., near-to-ground) imaging, the Shack-Hartmann (SH) wavefront sensor is commonly used, as it enables wavefront measurements on extended sources.

When performing wavefront measurements on an extended scene, the angular decorrelation of the phase perturbation over the object's field of view can significantly affect the accuracy of the wavefront estimation. The impact of this phenomenon, known as anisoplanatism, on SH wavefront sensing has been studied through analytical developments and end-to-end simulations.[1,2] Their work proposed an analytical expression for the SH measurement error induced by anisoplanatism in the Rytov regime. While this anisoplanatism measurement error has been validated by numerical simulations, it has yet to be experimentally tested under endo-atmospheric conditions. The realization of this experimental validation requires knowledge of the turbulence strength along the line of sight, specifically the C_n^2 profile.

In this paper, we present an experimental characterization of the C_n^2 profile using SH data in near-ground horizontal observation conditions. Our approach is based on the SCO-SLIDAR method,[3] which estimated the C_n^2 profile from the numerical inversion of a direct model that describes the spatial correlations of slope and intensity measurements in the Rytov regime. This method has been previously validated for slant-path propagation.[4,5] Here, we exploit multi-directional SH slope and intensity measurements to retrieve a C_n^2 profile for each analysis

Further author information:
Yann Lai-Tim: E-mail: yann.lai-tim@onera.fr, Telephone:+33 (0)1 46 73 43 83
Nicolas Védrenne: E-mail: nicolas.vedrenne@onera.fr, Telephone: +33 (0)1 46 73 47 57

Unconventional Imaging, Sensing, and Adaptive Optics 2025, edited by Jean Dolne, Santasri Bose-Pillai, Matthew Kalensky, Proc. of SPIE Vol. 13619, 136190J · 2025 Published by SPIE
0277-786X · doi: 10.1117/12.3065744

direction using the SCO-SLIDAR technique.[3] The outline of this paper is as follows: Section 2 introduces the formalism of SCO-SLIDAR. Section 3 describes the experimental field campaign and the data extraction steps. Finally, in Section 4, we present the measurement results.

2. FORMALISM

In this Section, we present the formalism of the SCO-SLIDAR approach in the context of near-ground C_n^2 profiling over a finite distance.

Let us assume that a Shack-Hartmann wavefront sensor (SHWFS) measures the wavefront coming from a point source at a distance L from the sensor. It delivers a set of wavefront slopes and intensities per subaperture. At each frame, the slope computed on the m^{th} subapertures focal image is a 2-D vector $\boldsymbol{s}_m$ with two components, along the k axis ($k \in x, y$). The point source intensities on the m^{th} subaperture is denoted i_m. For every sub-aperture, the normalized intensity fluctuation δi_m is defined as $\delta i_m = \frac{i_m - o_m}{o_m}$ where $o_m =< i_m >$ is the time-averaged intensity. In practice, o_m is evaluated by computing the empirical average $\frac{1}{N}\sum_{t=1}^{N} i_{m,t}$ where N is the number of frames and t is the frame index.

Slope correlations, $\langle s_m^k s_n^l \rangle$, between sub-apertures m and n, intensity fluctuation correlations $\langle \delta i_m \delta i_n \rangle$ and their coupling, $\langle \delta i_m s_n^l \rangle$ can be linearly related to C_n^2 assuming the weak perturbation approximation:[1,3]

$$\langle s_m^k s_n^l \rangle = \int_0^L C_n^2(z) W_s^{kl}(z, \boldsymbol{d}_{mn}) dz, \tag{1}$$

$$\langle \delta i_m \delta i_n \rangle = \int_0^L C_n^2(z) W_i(z, \boldsymbol{d}_{mn}) dz, \tag{2}$$

$$\langle s_m^k \delta i_n \rangle = \int_0^L C_n^2(z) W_{si}^k(z, \boldsymbol{d}_{mn}) dz. \tag{3}$$

where z is the distance from the observer along the line of sight and L is the propagation distance. W_s^{kl}, W_i and W_{si}^k are weighting functions defined, in the spherical wave case, by:[6]

$$W_s^{kl}(z, \boldsymbol{d}_{mn}) = (2\pi k_0 D)^2 \, \mathrm{FT}^{-1}[f_k f_l \; W_\varphi^{z_e}(\boldsymbol{f}) \left(\frac{z_e}{z}\right)^2 \cos^2(\pi z_e \lambda \|\boldsymbol{f}\|^2) \;\; \widetilde{P}^2(\boldsymbol{f})](\boldsymbol{d}_{mn}) \tag{4}$$

$$W_i(z, \boldsymbol{d}_{mn}) = 4 \, \mathrm{FT}^{-1}[\; W_\varphi^{z_e}(\boldsymbol{f}) \left(\frac{z_e}{z}\right)^2 \; \sin^2(\pi z_e \lambda \|\boldsymbol{f}\|^2) \; \widetilde{P}^2(\boldsymbol{f})](\boldsymbol{d}_{mn}) \tag{5}$$

$$W_{si}^k(z, \boldsymbol{d}_{mn}) = 4\pi k_0 \Re \left[i \, \mathrm{FT}^{-1}[f_k \; W_\varphi^{z_e}(\boldsymbol{f}) \left(\frac{z_e}{z}\right)^2 \; \sin(\pi z_e \lambda \|\boldsymbol{f}\|^2) \; \cos(\pi z_e \lambda \|\boldsymbol{f}\|^2) \; \widetilde{P}^2(\boldsymbol{f})](\boldsymbol{d}_{mn}) \right] \tag{6}$$

where $k_0 = 2\pi/\lambda$ is the wave number, $z_e = \frac{L}{L-z} z$ is the equivalent distance in the case of spherical wave propagation, D is the sub-aperture size, $\mathrm{FT}^{-1}[.]$ stands for the inverse Fourier transform with respect to the spatial frequency $\boldsymbol{f} = (f_x, f_y)$, $\boldsymbol{d}_{mn} = \boldsymbol{r}_m - \boldsymbol{r}_n$ is the separation vector between the considered subapertures, $\boldsymbol{r}_m$ being the position of sub-aperture m in the pupil plane, $\widetilde{P}$ stands for the Fourier transform of the sub-aperture spatial averaging and $W_\varphi^{z_e}$ is a modified Von-Kármán spectrum defined as follows:

$$W_\varphi^{z_e}(\boldsymbol{f}) = 0,033 k_0^2 (2\pi)^{-\frac{2}{3}} \left[\|\boldsymbol{f}\|^2 + \left(L_0 \frac{z_e}{z}\right)^{-2} \right]^{-\frac{11}{6}} \exp\left(- \left(\frac{2\pi l_0 \frac{z_e}{z}}{5.91} \right)^2 \|\boldsymbol{f}\|^2 \right). \tag{7}$$

In Eq. (7) L_0 and l_0 are respectively the outer and inner scale of turbulence.

Assuming a discrete description of the turbulence profile, denoted $\boldsymbol{S}$, the concatenation of the correlations given in Eqs. (1-3) into a single vector $\boldsymbol{C}$ is related to $\boldsymbol{S}$ according to:

$$\boldsymbol{C} = M\boldsymbol{S}, \tag{8}$$

where M is a matrix whose column vectors are filled using the weighting functions of Eqs. (4-6). To recover the C_n^2 profile, SCO-SLIDAR principle consists in solving the direct problem described by Eq. (8). To do so, $\boldsymbol{C}$ is estimated empirically from a finite number of recorded frame. The corresponding vector of estimated correlations is denoted $\boldsymbol{C}_{mes}$. Taking into account the different noise sources affecting $\boldsymbol{C}_{mes}$ Eq. (8) can be rewritten:

$$\boldsymbol{C}_{mes} = M\boldsymbol{S} + \boldsymbol{C_d} + \boldsymbol{u}, \tag{9}$$

where $\boldsymbol{C_d}$ is the covariance vector of the noises affecting slope and intensity measurements; $\boldsymbol{u}$ the convergence noise related to the finite number of data, which we assume to be Gaussian. Assuming that the system is well calibrated, it is possible to completely determine $\boldsymbol{C_d}$[7] and to define an unbiased estimation of the covariance vector, $\hat{\boldsymbol{C}}_{mes} = \boldsymbol{C}_{mes} - \boldsymbol{C_d}$. Thus, the direct problem can be rewritten as:

$$\hat{\boldsymbol{C}}_{mes} = M\boldsymbol{S} + \boldsymbol{u}, \tag{10}$$

A sampled estimate of C_n^2, $\hat{\boldsymbol{S}}$ is finally retrieved from the inversion of Eq. (10) using a maximum-likelihood approach, under positivity constraint (as C_n^2 is never negative). $\hat{\boldsymbol{S}}$ minimizes the following criterion:

$$J(\boldsymbol{S}) = (\hat{\boldsymbol{C}}_{mes} - M\boldsymbol{S})^T C_{conv}^{-1} (\hat{\boldsymbol{C}}_{mes} - M\boldsymbol{S}) \tag{11}$$

where $C_{conv} = \langle \boldsymbol{u}\boldsymbol{u}^T \rangle$ is the covariance matrix of $\boldsymbol{u}$, the convergence noise.

3. EXPERIMENT

3.1 Localization

The C_n^2 profile experimental characterization took place at ONERA's site in Fauga-Mauzac, near Toulouse, southern France, in April 2024. Figure 1 shows the experimental setup. A horizontal line of sight of 1040 meters separates building X1, where the Shack-Hartmann wavefront sensor (SHWFS) was installed, from building X2, where the source module was located.

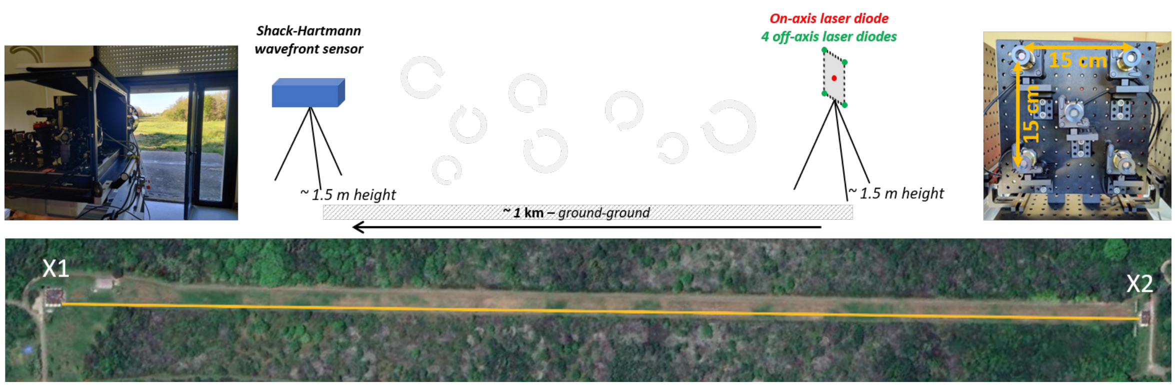

Figure 1. Experimental campaign at ONERA's site in Fauga-Mauzac.

3.2 Experiment design

In building X1, the SHWFS is coupled to a Cassegrain telescope with a diameter $D = 0.35m$ and a central obscuration of $0.23D$. SHWFS images consist of 8×8 square subapertures, each with 20×20 pixels. In the pupil plane, the size of the sub-aperture is 4.375 cm. The image at the micro-lenses' focal plane is recorded with a C-RED 3 camera (Oxford Instruments - Andor) using a 160×160 pixels region of interest (ROI) with a framerate of 250 Hz and an exposure time of 2 ms. The exposure time has been chosen to be lower than the coherence time of the turbulence, which was expected to be approximately 10 ms for the experimental line of sight.

In building X2, the source module is composed of five 1550 nm laser diodes. As illustrated in Figure 1, the laser diodes are separated into two groups: a single on-axis laser diode (shown in red) and four off-axis laser diodes (depicted in green), which collectively form a square with a side length of 15 cm. The purpose of this design is to allow the experimental measurement of the anisoplanatism measurement error,[2] by alternatively acquiring SHWFS data on a point source using the on-axis diode and SHWFS data on an extended scene using the off-axis diodes, under the same turbulence conditions. In this paper, we focus on exploiting these SHWFS data to perform C_n^2 profiling. The estimated C_n^2 profiles will be used later to experimentally validate the anisoplanatism measurement error, which will be discussed in a future paper.

During this campaign, an anemometer was deployed between X1 and X2 and provided wind velocity measurements.

3.3 Data exploitation

In the following, we use the SHWFS images acquired on April 25, 2024 at 7:36 p.m (local time) to estimate the C_n^2 along the line of sight.

3.3.1 Data presentation

The data consists of a sequence of 8000 SHWFS images, acquired at 250 Hz with an exposure time of 2 ms. The SHWFS camera and the laser diodes were synchronized so that each even frame captured a single on-axis point-source SHWFS image, while each odd frame captured from four off-axis point-sources. Figure 2 shows two consecutive SHWFS images. Each source's power was adjusted to have a satisfactory Signal-to-Noise Ratio in the SHWFS images ($SNR \approx 30$) while preventing SHWFS camera saturation during data acquisition.

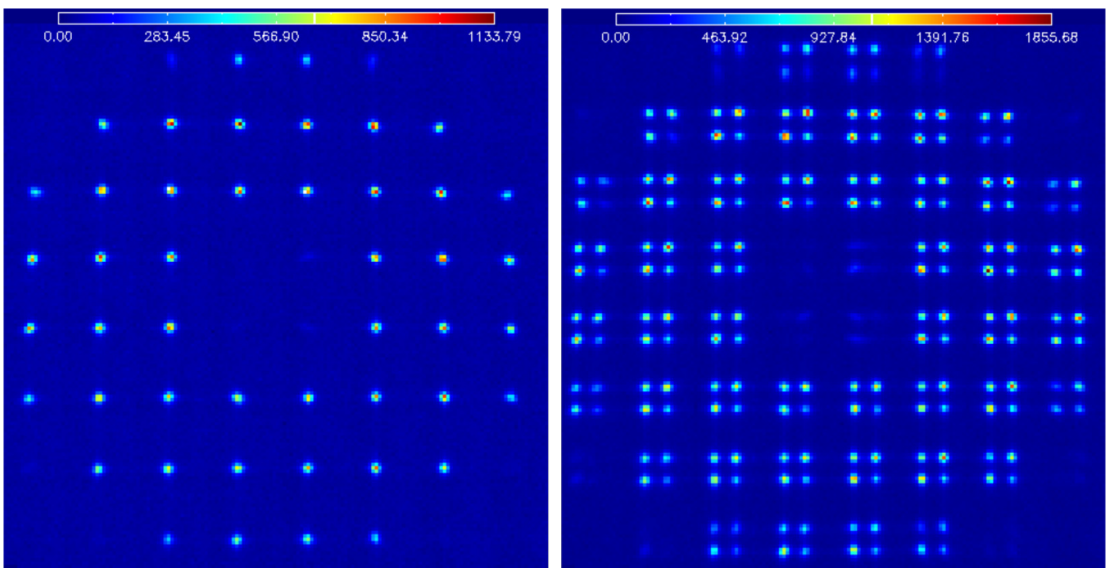

Figure 2. Example of two consecutive SHWFS images, corresponding to the point-source configuration on the left and to the extended-scene configuration on the right. The pixel values, displayed on the color bar, are in units of camera Analog-to-Digital Units (ADU).

For processing purposes, the sequence of 8000 SHWFS images is split into two subsets of 4000 images each. The first subset, labeled A, contains the even-indexed frames acquired from the on-axis point source, while the second subset, labeled B, contains the odd-indexed frames captured from the quadruple point sources.

The wind speed was very low during the measurements ($< 0.3m/s$). As a result, we observed that the phase correlation time was significantly longer than the delay between two consecutive frames. Consequently, among the 4000 measured SH slopes in each subset, only about 100 measurements were fully decorrelated. It should be noted that, due to the limited number of decorrelated phase measurements, this dataset is not intended for an accurate evaluation of the turbulence profile and characteristics. Instead, its primary purpose is to correctly reproduce and investigate the angular decorrelation introduced by anisoplanatism, which is what the experiment was designed for. Nevertheless, here we exploit this dataset to assess the reliability of the SCO-SLIDAR method for estimating C_n^2 profiles under near-ground horizontal observation conditions.

3.3.2 Slope and intensity measurements

Before processing the data to extract slope and intensity measurements required for the C_n^2 profiling, each subset is pre-processed as follows:

1. A background image is subtracted from each image. The background image correponds to the SHWFS image captured with the laser diodes switched off, just before the data acquisition.
2. The gain map of the SHWFS camera is applied to each image to account for the heterogeneous pixel response of the sensor. The intensity of the resulting equalized images is then expressed in photo-electrons (phe^-).

For each frame and each subaperture of the SH, the slope and intensity measurements are performed for each spot on the SH focal image. Since we use five laser diodes, there are five point-source directions to consider, as shown in Figure 3. We denote the measurement direction as θ: $\theta = 0$ corresponds to the on-axis spot from subset A while $\theta \in \{1, 2, 3, 4\}$ corresponds to one of the off-axis spots from subset B. The angular separation between the on-axis spot and each off-axis spot is $(|\theta_x|, |\theta_y|) = (100, 100)$ μrad in absolute value.

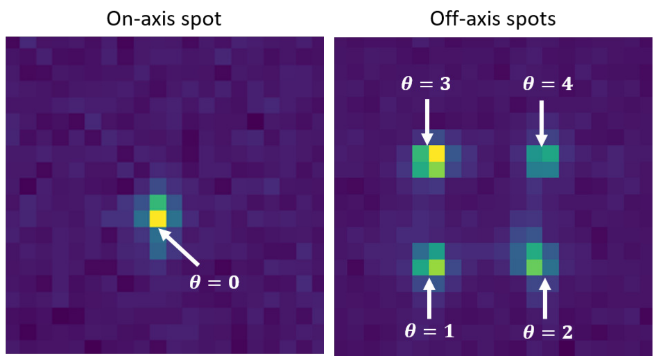

Figure 3. Examples of a SH focal image from subset A (on the left) and from subset B (on the right).

For the m^{th} subaperture at frame t, the slope in direction θ is computed iteratively using the Weighted Center of Gravity (WCOG) algorithm.[8] At iteration p, the x-slope is computed using the following formula:

$$(\hat{s}^x_{m,\theta,t})^{(p)} = \frac{\sum_{i,j} \boldsymbol{x}[i,j]\boldsymbol{W}^{(p)}[i,j]\boldsymbol{I}_{m,\theta,t}[i,j]}{\sum_{i,j} \boldsymbol{W}^{(p)}[i,j]\boldsymbol{I}_{m,\theta,t}[i,j]} \tag{12}$$

where:

- $\boldsymbol{x}$ is the x-coordinate map of the 20×20 pixel subaperture grid,
- (i, j) are the pixel coordinates in the m^{th} subaperture frame,
- $\boldsymbol{W}^{(p)}$ is a 20×20 pixel 2-D Gaussian weighting map with a 3-pixel Full-Width at Half Maximum (FWHM). Its maximum value is 1 and its center is the 2-D slope estimated at the previous iteration step (p-1), denoted as $(\hat{\boldsymbol{s}}_{m,\theta,t})^{(p-1)}$,
- $\boldsymbol{I}_{m,\theta,t}$ is the 20×20 pixel intensity map of the m^{th} SH subaperture at frame t. This map comes from subset A if $\theta = 0$ (on-axis source) and from subset B otherwise.

For the first iteration, we made a rough initial estimate of the spot position in direction θ from the time-average SHWFS image through visual inspection. We then initialized the center of the Gaussian weighting map at this position. We set the number of iteration steps to $K = 20$ and we confirmed that this was sufficient to ensure proper convergence of the WCOG algorithm. The y-slope is obtained by substituting the x-coordinate map with the y-coordinate map in Eq. (12).

Initial slope values for the WCOG algorithm could also be determined via a WCOG estimation on the time-average SHWFS image, utilizing a circular window as weighting map. This window would be centered on the spot at direction θ (to the nearest pixel) with a radius equal to the size of the time-average spot.

The intensity in direction θ at frame t on the m^{th} subaperture is computed as follows:

$$\hat{i}_{m,\theta,t} = \sum_{i,j} \boldsymbol{W}[i,j]\boldsymbol{I}_{m,\theta,t}[i,j] \tag{13}$$

where $\boldsymbol{W}[i,j]$ is a 2-D Gaussian weighting map with a 3-pixel FWHM centered at the final estimated slope position $(\hat{\boldsymbol{s}}_{m,\theta,t})^{(K)}$.

The FWHM of the Gaussian map was chosen to effectively extract pixels belonging to the relevant spot while filtering out contributions from other spots. Through numerical simulations, we found that a 3-pixel FWHM provides accurate slope and intensity measurements.

3.3.3 Turbulence parameters measurement

The Fried parameter r_0, and the log-amplitude variance, σ_χ^2, can be estimated directly from the SH data, thereby providing a way to validate the turbulence conditions.

The Fried parameter r_0, at the source wavelength ($\lambda = 1.55\mu m$) is estimated directly from the SH slopes.[9] To do so, we first compute the wavefront phases from the SH slopes. We then project these phases onto the 44 first Zernike modes (excluding the piston mode) and fit an $n^{(-11/3)}$ power law to the phase variance for the modes with a radial order $2 \leq n \leq 5$. We exclude higher radial orders ($n > 5$) from the fit because their reconstructed Zernike variances are corrupted by aliasing and a lower SNR. Tip and tilt are also excluded because they can be influenced by telescope vibrations, which would bias the r_0 estimation. Due to the altitude of the line of sight and the small size of the telescope, the influence of the outer scale, L_0, is very small. Additionally, the influence of accurate knowledge of the inner scale, l_0, is negligible due to the size of the sub-apertures (4.375 cm). We therefore assume $L_0 = 20$ m and an inner scale $l_0 = 5$ mm. The average r_0 estimated from the slope data is 0.065 m.

The scintillation index, σ_i^2, is a measure of the intensity fluctuations and is estimated directly from the SH intensity measurements using the relationship $\sigma_i^2 =< (\delta i_m)^2 >$ where δi_m is the normalized intensity fluctuation. We verified that the scintillation indices for all source directions were well below the Rytov limit of 1.2. This confirms that the weak perturbation approximation is valid for our measurements. We then estimate the log-amplitude variance, σ_χ^2, by fitting a log-normal probability distribution to the histogram of the intensity measurements $(\hat{i}_{m,\theta,t})_t$ for each direction θ and subaperture m. The resulting average log-amplitude variance is 0.033. It should be noted that SH intensities are measured over a finite aperture size. Here, we neglect the influence of pupil averaging on intensity measurements and approximate the log-amplitude variance by its average value over the subaperture size.

4. RESULTS

4.1 Measured profiles

The C_n^2 profiles for each source direction θ are retrieved using the SCO-SLIDAR method,[3] presented in Section 2. Figure 4 shows the results obtained for each of the source directions. The C_n^2 profiles are discretized by assuming five equi-distant turbulence layers, each with a thickness of 200 m, within which the C_n^2 value is constant. The dotted brown line represents the average C_n^2 profile across all five directions.

We observe that three main turbulence layers can be identified. The first is located between 0 and 200 m from the telescope with an average C_n^2 of $4.6 \times 10^{-14} m^{-2/3}$; the second is located between 400 and 600 m with an average C_n^2 of $3.3 \times 10^{-14} m^{-2/3}$; and the third is located between 800 and 1000 m with an average C_n^2 of $2.7 \times 10^{-14} m^{-2/3}$.

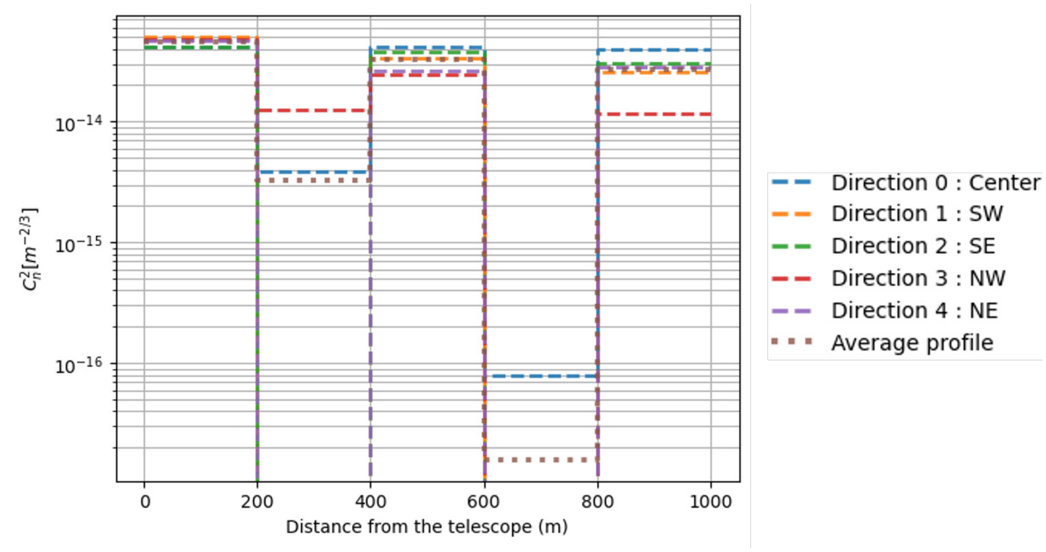

Figure 4. Estimated C_n^2 profiles.

4.2 Comparison to turbulence parameters

The Fried parameter r_0 and the log-amplitude variance σ_χ^2 can be estimated in two ways. On one hand, they can be directly computed from the SH slopes and intensities, processed separately, as described in Section 3.3.3. On the other hand, they can be calculated in a framework that jointly processes SH slopes and intensities, by using analytical formulas[10,11] with the estimated C_n^2 profile measured by SCO-SLIDAR.

To assess the reliability of the inversion process, we compare the turbulence parameters obtained from the estimated C_n^2 profiles to the average Fried parameter and log-amplitude variance directly measured from the SH data. To quantify this comparison, we define the normalized error (NE) for both r_0 and σ_χ^2:

$$NE_{\mathrm{r}_0} = \frac{\sqrt{(\mathrm{r}_{0SCO} - \mathrm{r}_{0exp})^2}}{\mathrm{r}_{0exp}} \tag{14}$$

$$NE_{\sigma_\chi^2} = \frac{\sqrt{(\sigma^2_{\chi SCO} - \sigma^2_{\chi exp})^2}}{\sigma^2_{\chi exp}} \tag{15}$$

where r_{0SCO} and $\sigma^2_{\chi SCO}$ are the values computed using the C_n^2 profile from SCO-SLIDAR, and r_{0exp} and $\sigma^2_{\chi exp}$ are the values directly computed from the SH data.

Table 1. Fried parameters and log-amplitude variances obtained from the estimated C_n^2 profiles and normalized errors.

C_n^2 profile	$r_0[m]$	$NE_{r_0}[\%]$	σ_χ^2	$NE_{\sigma_\chi^2}[\%]$
Direction $\theta = 0$	0.068	3.8	0.040	25.0
Direction $\theta = 1$	0.066	2.0	0.028	11.5
Direction $\theta = 2$	0.070	8.1	0.033	0.3
Direction $\theta = 3$	0.065	0.5	0.023	27.8
Direction $\theta = 4$	0.071	8.5	0.026	19.0
Average profile	0.068	4.5	0.030	6.0

Table 1 presents the r_{0SCO} and $\sigma^2_{\chi SCO}$ values estimated for each of the turbulence profiles along with their corresponding normalized errors. For all the C_n^2 profiles, we observe that the normalized error for r_0 is below 10%, and for σ^2_χ, it is below 30%, which demonstrates reasonable consistency between the two approaches.

The normalized error is, on average, greater for σ^2_χ than for r_0. This could be attributed to the influence of noise, residual background and aperture function on flux measurements, as their biases have not been removed. Further investigations are needed to better understand this phenomenon.

Overall, a satisfactory concordance between the two evaluations of the turbulence parameters is demonstrated here. This consistency is explained by the fact that both estimation methods use the same SH slope and intensity data, processed either separately for r_{0exp} and $\sigma^2_{\chi_{exp}}$, or jointly for r_{0SCO} and $\sigma^2_{\chi SCO}$. It confirms the reliability of the SCO-SLIDAR method for performing C_n^2 profiling under near-ground, horizontal line-of-sight conditions.

5. CONCLUSION

In this paper, we carried out C_n^2 profiling from Shack-Hartmann measurements under near-ground horizontal observation conditions. We used multi-directional SH slope and intensity measurements, obtained from five point sources, to estimate the C_n^2 profile for each analysis direction. The turbulence profiles were retrieved using the SCO-SLIDAR method.[3]

Macroscopic turbulence parameters, r_0 and σ^2_χ, estimated from the measured C_n^2 show good agreement with direct measurements on the SH data. The strong agreement on r_0 demonstrates that the technique delivers a realistic estimation of the integral of the profile, while the good agreement on σ^2_χ indicates a correct estimation of distant turbulent layers. These observations give us good reasons to use the estimated C_n^2 profiles for the experimental validation of anisoplanatism error, which we plan to cover in a future publication.

The SCO-SLIDAR approach is based on the weak perturbation Rytov regime. This assumption no longer holds in strong turbulence condtions. The reconstructed C_n^2 profiles presented here were obtained under moderate turbulence conditions with a near-ground horizontal line of sight. Future work will focus on investigating limitations of the SCO-SLIDAR method under stronger turbulence conditions, incorporating comparisons with alternative C_n^2 profiling techniques from Shack-Hartmann data, such as SLODAR[12] and CO-SLIDAR.[3]

REFERENCES

[1] Robert, C., Conan, J.-M., Michau, V., Fusco, T., and Vedrenne, N., "Scintillation and phase anisoplanatism in Shack-Hartmann wavefront sensing," *J. Opt. Soc. Am. A, JOSAA* **23**, 613–624 (Mar. 2006).

[2] Védrenne, N., Michau, V., Robert, C., and Conan, J.-M., "Shack-Hartmann wavefront estimation with extended sources: anisoplanatism influence," *J. Opt. Soc. Am. A, JOSAA* **24**, 2980–2993 (Sept. 2007).

[3] Védrenne, N., Michau, V., Robert, C., and Conan, J.-M., "Cn2 profile measurement from Shack-Hartmann data," *Optics Letters* **32**, 2659–2661 (Sept. 2007).

[4] Védrenne, N., Montmerle, A. B., Robert, C., Michau, V., Montri, J., and Fleury, B., "Cn2 profile measurement from Shack-Hartmann data: Experimental validation and exploitation," in [*Optics in Atmospheric Propagation and Adaptive Systems XIII*], Stein, K. and Gonglewski, J. D., eds., **7828**, 78280B, SPIE / International Society for Optics and Photonics (2010).

[5] Bonnefois, A. M., Velluet, M.-T., Cissé, M., Lim, C. B., Conan, J.-M., Petit, C., Sauvage, J.-F., Meimon, S., Perrault, P., Montri, J., and Védrenne, N., "Feasibility demonstration of AO pre-compensation for GEO feeder links in a relevant environment," **30**(26), 47179–47198.

[6] Sauvage, C., Robert, C., Mugnier, L. M., Conan, J.-M., Cohard, J.-M., Nguyen, K.-L., Irvine, M., and Lagouarde, J.-P., "Near ground horizontal high resolution $Cn2$ profiling from Shack–Hartmann slopeand scintillation data," *Applied Optics* **60**, 10499–10519 (Dec. 2021).

[7] Roddier, F., ed., [*Adaptive Optics in Astronomy*], Cambridge University Press, Cambridge (1999).

[8] Nicolle, M., Fusco, T., Rousset, G., and Michau, V., "Improvement of Shack–Hartmann wave-front sensor measurement for extreme adaptive optics," *Optics Letters* **29**, 2743–2745 (Dec. 2004).

[9] Fusco, T., Rousset, G., Rabaud, D., Gendron, E., Mouillet, D., Lacombe, F., Zins, G., Madec, P.-Y., Lagrange, A.-M., Charton, J., Rouan, D., Hubin, N., and Ageorges, N., "NAOS on-line characterization of turbulence parameters and adaptive optics performance," *Journal of Optics A: Pure and Applied Optics* **6**, 585 (Apr. 2004).

[10] Frieden, B. R., "Optical Transfer of the Three-Dimensional Object*†," *JOSA* **57**, 56–66 (Jan. 1967).

[11] Fried, D. L., "Anisoplanatism in adaptive optics," *JOSA* **72**, 52–61 (Jan. 1982).

[12] Wilson, R. W., "SLODAR: Measuring optical turbulence altitude with a Shack–Hartmann wavefront sensor," *Monthly Notices of the Royal Astronomical Society* **337**, 103–108 (Nov. 2002).